Surface Science xxx (2015) xxx–xxx

Contents lists available at ScienceDirect

Surface Science

journal homepage: www.elsevier.com/locate/susc

Extreme UV induced dissociation of amorphous solid water and crystalline water bilayers on Ru(0001)

Feng Liu *, J.M. Sturm, Chris J. Lee, Fred Bijkerk

MESA + Institute for Nanotechnology, University of Twente, Enschede, The Netherlands

ARTICLE INFO

Available online xxxx

Keywords:
Water
EUV
Ruthenium
Dissociation
Secondary electron
Reaction cross section

ABSTRACT

The extreme ultraviolet (EUV, $\lambda = 13.5$ nm) induced dissociation of water layers on Ru(0001) was investigated. We irradiated amorphous and crystalline water layers on a Ru crystal with EUV light, and measured the surface coverage of remaining water and oxygen as a function of radiation dose by temperature programmed desorption (TPD). The main reaction products are OH and H with a fraction of oxygen from fully dissociated water. TPD spectra from a series of exposures reveal that EUV promotes formation of the partially dissociated water overlayer on Ru. Furthermore, loss of water due to desorption and dissociation is also observed. The water loss cross sections for amorphous and crystalline water are measured at $9 \pm 2 \times 10^{-19}$ cm^2 and $5 \pm 1 \times 10^{-19}$ cm^2, respectively. Comparison between the two cross sections suggests that crystalline water is more stable against EUV induced desorption/dissociation. The dissociation products can oxidize the Ru surface. For this early stage of oxidation, we measured a smaller (compared to water loss) cross section at 2×10^{-20} cm^2, which is 2 orders of magnitude smaller than the photon absorption cross section (at 92 eV) of gas phase water. The secondary electron (SE) contributions to the cross sections are also estimated. From our estimation, SE only forms a small part (20–25%) of the observed photon cross section.

1. Introduction

Since light with a shorter wavelength can provide better imaging resolution, Extreme ultraviolet (EUV) light, with a wavelength of 13.5 nm, has been chosen for the current generation of high-end photolithography system [1,2]. However, EUV light is strongly absorbed by all materials. Therefore, EUV imaging systems operate in vacuum, and require reflective optics. Photochemical reactions can then occur on the surface of the reflective optics. With a photon energy well above the dissociation energy of water [3], EUV and EUV-induced low energy secondary electrons (SE) readily dissociate water adsorbed at the mirror surface. The dissociation products can cause surfaces of mirrors to oxidize, degrading imaging performance and throughput. To protect EUV optics against oxidation, several metal and metal oxide capping layers have been proposed [4]. The resilience of these capping layers has usually been studied using electron impact (EI) as a proxy for EUV radiation [5–7]. Unfortunately, electrons do not fully emulate the near-surface conditions generated during an EUV light pulse, leaving the relevance of these experiments an open question [4,7,8]. For selecting the right capping material and to predict accurately mirror's long term performance, we need to study the photochemistry at water–metal interfaces under realistic conditions.

Ruthenium is a candidate material for capping EUV optics to protect them from performance degradation due to carbon growth and oxidation [4]. It has been demonstrated that the water/Ru interface is very sensitive to both soft X-rays and low energy electrons. Hydroxyl groups were found on the Ru surface after short exposure to soft X-rays [9] and electrons [6]. Because oxygen up to monolayer coverage desorbs at a relatively high temperature (above 1100 K for Ru) [10], after long exposures, atomic oxygen from dissociated water can accumulate to form an oxide that may penetrate several nanometers under the surface [7]. Electron irradiation studies, on the other hand, found no direct evidence for atomic oxygen on the surface [6]. These differences highlight the need for EUV irradiation studies in preference to electron irradiation studies, and for the early stages of surface oxidation to be more carefully investigated.

Unlike photochemistry in the visible and the UV range [11], SE from EUV excited substrate are highly relevant for the surface reactions. In order to put both photon and SE induced processes into perspective, comparison should be made between their cross sections. However, cross section data for EUV induced dissociation is still lacking. A well defined surface, such as the Ru(0001) surface, is essential for a comparable cross section measurement. Therefore, we revisit the well-known water/Ru interface and explore how it reacts under EUV conditions.

The unique interplay between water–water and water–Ru interactions makes the water/Ru(0001) interface an interesting system to be studied. Depending on adsorption temperature, deposition geometry, and flux, water clusters and aggregates can form [12]. Amorphous

* Corresponding author.
E-mail address: F.Liu-2@utwente.nl (F. Liu).

http://dx.doi.org/10.1016/j.susc.2015.09.009
0039-6028/

solid water (ASW) and crystalline water bilayers (CWB) are two intact water structures that can be grown on a Ru surface. Crystalline water wets the Ru surface at 150 K, while ASW has a less ordered structure and remains physisorbed. Most importantly, CWB has a bilayer geometry [13], while ASW consists of three dimensional structures, such as clusters [12]. As water molecules form strong hydrogen bonds, the hydrogen networks inside the two water structures are also intrinsically different. Theoretically, it has been shown that dissociation barrier of water on Ru depends on structure [14]. However, it is still an open question how the structural difference and wetting influence water dissociation under EUV conditions. We will address this structural dependency by comparing EUV induced dissociation of ASW and CWB.

Apart from the intactly adsorbed layers, water can form the partially dissociated overlayer ($H_2O + OH$) on Ru(0001) surface, which is also the most stable adsorption state on Ru(0001) [6,9,14,15]. Both intact and dissociative adsorption layers are well distinguishable in temperature programmed desorption (TPD). Their coverages are also given by the corresponding TPD peak area. On the other hand, reduction in the integrated TPD area indicates dissociation/desorption of water. The atomic oxygen created by the complete dissociation of water will adsorb on Ru crystal surfaces [16]. The adsorbed oxygen can be removed by heating to 1550 K. The desorbed oxygen can be detected by a mass spectrometer to provide surface oxygen coverage [16,17].

In this paper, the results of studies on the EUV-induced dissociation of ASW and CWB on a Ru(0001) surface, along with the subsequent oxidation of the Ru(0001) surface are presented. We use TPD spectroscopy to determine water dissociation and oxidation cross sections for the Ru(0001) surface, which is a necessary first step for predicting degradation rates over longer terms and in an environment with more chemically active species present [10,16,17].

2. Methods

The experiments were performed in an ultra-high vacuum (UHV) chamber with base pressure of 3×10^{-10} mbar. The vacuum is achieved using a turbo molecular pump and a Titanium sublimation pump [18]. The chamber is equipped with a quadrupole mass spectrometer (QMS, Hiden HAL 301) for TPD measurements, and an ion gun for sample cleaning. A retractable quartz tube doser is used to dose the ruthenium sample with water, while minimizing the increase in background pressure.

The sample consisted of a circular ruthenium (0001) single crystal (Surface Preparation Laboratories, The Netherlands), mounted on a manipulator. The diameter of the crystal is 11 mm. The sample temperature is controlled via a combination of active heating to 1580 K, and liquid nitrogen cooling to 80 K. The temperature is monitored using a K-type thermocouple, spot-welded to the side of the crystal. The temperature of the crystal is controlled by a Eurotherm temperature controller, which is also used to provide a constant heating rate for the TPD measurements.

Water is very sensitive to surface impurities [15]. Therefore, special care is taken to limit the amount of surface carbon and oxygen. The crystal surface is prepared by first removing surface carbon through annealing in 2×10^{-8} mbar of O_2 at 1300 K, followed by repeated temperature cycling between 100 K and 1550 K to adsorb and desorb oxygen. The surface is then subjected to repeated cycles of Ar ion sputtering at 1 keV or 2 keV, followed by flash annealing to 1550 K [15,19]. This cleaning process is repeated until reference water TPD spectra [15,19] are consistently reproduced and no CO peak is observed above 800 K in the TPD spectra [4]. Between each subsequent measurement, the sample is flash annealed to 1550 K to remove remaining oxygen on the surface.

The sample is dosed with deionized water that has been further purified by freeze–pump–thaw cycles. During dosing, the doser tube is placed 1 cm away from the crystal surface to keep the chamber pressure as low as possible. The water coverage is computed from the integrated TPD signals, and calibrated against the saturation coverage dosed at a sample temperature of 160 K [19].

The EUV light is produced by a Xe discharge plasma light source (Philips), operating at a repetition rate of 500 Hz. The broad band light from the plasma is first focused by a ruthenium coated grazing incidence collector, then reflected by a Mo/Si multilayer mirror (Phystex, central wavelength 13.5 nm), and finally passes through a 200 nm thick Zr/Si multilayer spectral purity filter (SPF). Both Mo/Si multilayer mirror and SPF have spectral bandwidths centred at 13.5 nm EUV with full width half maxima of 0.5 nm and 2 nm, respectively. The EUV pulses reaching the sample have a duration of 120 ns, and an energy flux of 32 $\mu J/cm^2$. The beam diameter at the sample surface is 5 mm full width half maximum, resulting in an average intensity of 16 mW/cm^2.

During operation, the pressure in the EUV light source chamber reaches 2×10^{-3} mbar. However, the SPF can prevent the gas from the source chamber entering the main chamber. As a result of this isolation, the pressure in the main chamber can be maintained at 1×10^{-9} mbar during EUV exposure.

TPD spectra were measured by heating the sample at a constant rate, and recording the amount of desorption for several masses. To improve the signal-to-background ratio, the QMS is placed in a differentially pumped housing with a cone-shaped aperture (entrance diameter of 4 mm diameter), which is placed approximately 1 mm from the sample surface. This geometry ensures that the QMS signal is dominated by surface desorption products and not background residual gases. Water TPD spectra were obtained using a heating rate of 1 K/s over a temperature range of 80–500 K. The oxygen TPD spectra were measured at a heating rate of 5 K/s over a temperature range of 500–1570 K. The absolute value of the oxygen surface coverage is calibrated to the saturation value (0.5 ML) for $p(2 \times 1)$ oxygen overlayer obtained at 400 K with 2×10^{-8} mbar × 300 s back dosed oxygen [16,20,21].

3. Results

ASW and CWB were grown on Ru crystal by dosing water at 83 and 160 K respectively [9,15,22], and exposed to EUV. The resulting photochemical reactions are reconstructed through the changes in the post-irradiation TPD spectra.

In the TPD spectra, the desorption temperature of each desorption peak is related to the strength of the adsorbate–substrate binding, or the energy barrier for recombinative desorption in the case of partially dissociated water. Peaks at relatively higher temperature originate from the molecules which bind stronger with the surface [23]. Since the QMS intensity is proportional to the desorption rate, the integrated peak area is proportional to the surface coverage [23]. The TPD results are divided into two separate subsections for ASW and CWB.

3.1. TPD of ASW

As shown by the bottom trace in Fig. 1(a), before exposure to EUV, the ASW TPD shows three desorption peaks, which are the multilayer water peak, C, the molecular water peak, A2, and the partially dissociated water peak, A1 [6,15,19]. Fig. 1(a) also shows the changes to the water TPD spectra for different EUV doses. The most noticeable changes are the peak height variations in A1 and A2, which are more clearly seen in Fig. 2(a). In Fig. 2(a), the A2 and C peak are plotted as a sum of the two, since the sum gives the total amount of molecular water on the surface. As the EUV exposure dose increases, the A2 peak decreases, and the A1 peak starts to increase, which is similar to the electron radiated case [6]. By a dose of 7×10^{16} photons/cm^2, the A2 peak has almost vanished, while the A1 peak has grown substantially. This indicates that water, adsorbed directly to the Ru(0001) surface, is partially dissociated ($H_2O \rightarrow OH + H$) due to EUV exposure.

Furthermore, increases in EUV dose result in lower integrated TPD spectra (Fig. 2(a)), indicating that the total amount of remaining water is reduced. From Fig. 2(a), we see that the peaks change in two

Please cite this article as: F. Liu, et al., Surf. Sci. (2015), http://dx.doi.org/10.1016/j.susc.2015.09.009

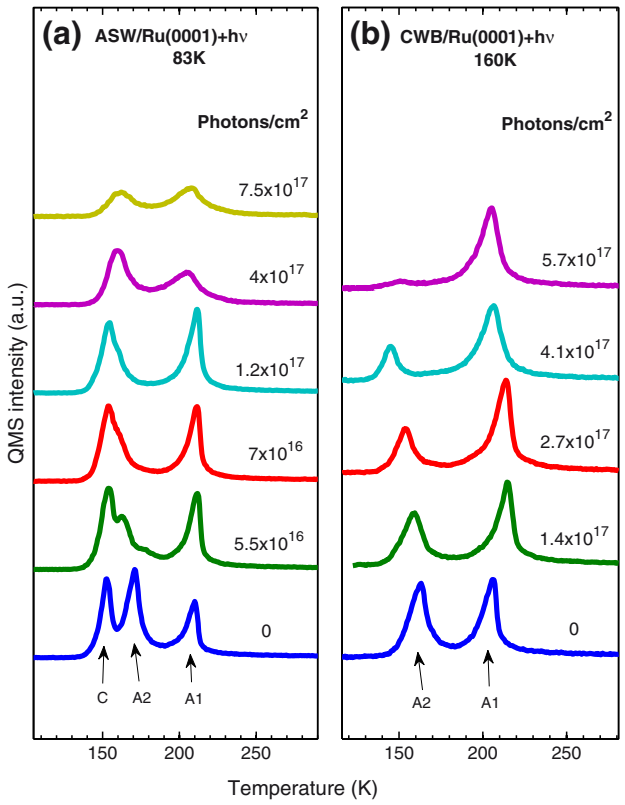

Fig. 1. Post-radiation TPD spectra (m/e = 18) of EUV irradiated ASW and CWB on Ru(0001). (a) 1 ML [16] ASW, (b) CWB. EUV doses are indicated above each corresponding TPD spectrum. The multilayer (C), molecular (A2) and partially dissociated (A1) water peaks are indicated for unexposed water TPD.

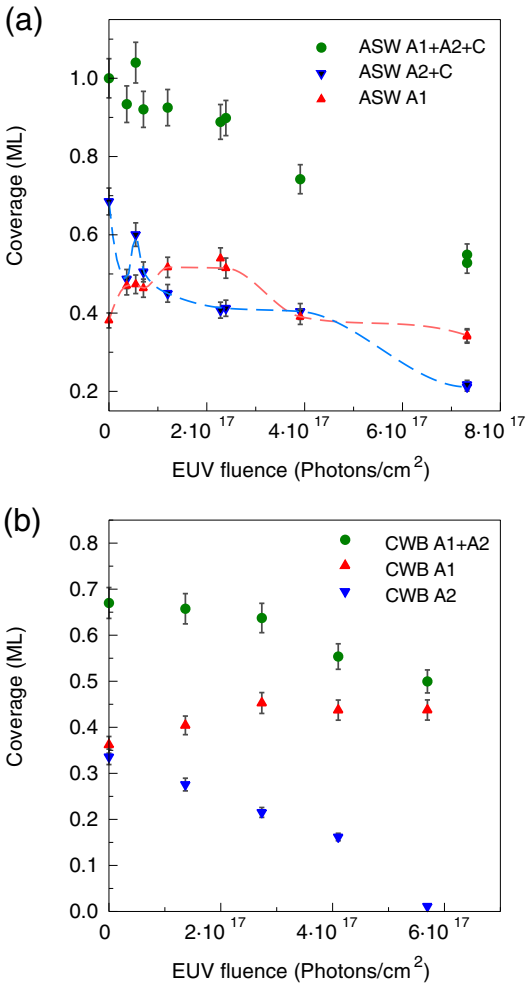

Fig. 2. Surface coverage of the A1, A2 and total TPD peak of ASW (a) and CWB (b) plotted against EUV dose. The coverage is normalized to the saturation coverage of CWB (0.67 ML) [13,15,24,25]. The dashed line is only a guide for the eye.

stages. In the initial stage with EUV doses up to 2.5×10^{17} photons/cm^2, a significant interchange between molecular and dissociated water is revealed by the difference in A2 + C and A1 peak areas. In the second stage, both molecular water and dissociated water reduce. However, although the total amount of water remaining on the surface decreases by 42% between exposures of 2.5×10^{17} photons/cm^2 and 7.5×10^{17} photons/cm^2, the A1 peak shows only a 35% reduction. Instead, the reduction of water appears to come mostly from the C/A2 peak. Furthermore, during all exposures, the A1 peak saturates just above 0.5 ML at 2.5×10^{17} photons/cm^2 with about 0.4 ML of intact multilayer/molecular water still on the surface. More exposure does not result in a higher coverage of partially dissociated water after the A1 peak has been saturated. Interestingly, the A1 peak did not reach the maximum A1 coverage (0.59 ML) obtained by O co-adsorption reported in Ref. [15]. Although the EUV-induced dissociation is not kinetically limited [14], a slower diffusion rate at 83 K could be a limiting factor in this case. A recent STM study [26] reveals that, due to strong H-bonding, it requires 30 min annealing at 145 K for the high-lying (multilayer) intact water to diffuse and rearrange to form the complete partially dissociated layer. As we see in Fig. 2(a), A1 peak saturates at 2×10^{17} photons/cm^2, which is about 2 min of exposure. Before A1 saturates, the remaining water in the multilayer may not diffuse fast enough to be chemisorbed and dissociated. Therefore, the A1 peak did not reach the maximum coverage. On the other hand, because the slow diffusion at 83 K restricts intermixing between the high-lying and low-lying water molecules [26], this allows us to make an estimation on the maximum coverage of the low-lying water for 1 ML ASW coverage, assuming all the low-lying water can be converted to partially dissociated water. This upper limit is set at 0.5 ML according to the saturation coverage of the A1 peak.

The peak area changes are also accompanied by small shifts in the peak positions. The peak temperature is plotted as a function of fluence in Fig. 3. For ASW, at low fluence (up to 2.5×10^{17} photons/cm^2), the A2 peak shifts from 171 K to 164 K before it is completely merged with the C peak, and A1 shifts from 210 K to 212 K. At higher dose (from 2.5×10^{17} photons/cm^2 to 7.5×10^{17} photons/cm^2), the multilayer peak C and the A2 peak is replaced by a new peak around 161.7 K, which is very close to the lowest A2 peak temperature seen at

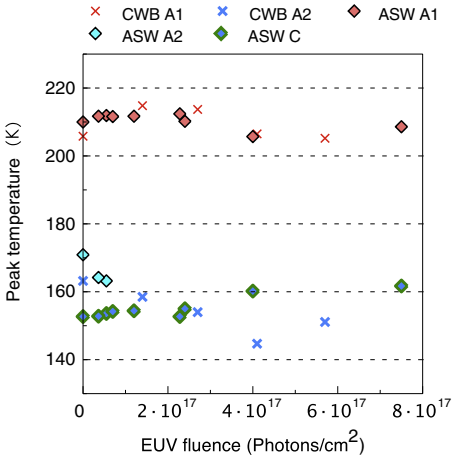

Fig. 3. A1, A2 and C peaks temperature of ASW and CWB plotted against EUV dose.

Please cite this article as: F. Liu, et al., Surf. Sci. (2015), http://dx.doi.org/10.1016/j.susc.2015.09.009

163.2 K. Meanwhile, the A1 peak shifts to a lower desorption temperature (from 210 to 208 K). Similar peak shifts are also obtained in the irradiated crystalline water dosed at 160 K (see Fig. 3).

The observed TPD peak shifts can be analysed to provide useful information on binding energy and coverage in the EUV exposed water layer [27]. However, the difficulty in this analysis is that the binding energy cannot be assumed to be coverage independent for water. As we see in Figs. 1 and 2, the shifts of the TPD peaks are accompanied by a change of the total water coverage. Therefore, we compared our results to reference TPD spectra with multiple coverages [19], and look for similarities in the peak shift trends. Based on this comparison we can conclude that the shifts of the A1 and A2 peaks can be well associated with increased coverage of partially dissociated water on the surface. They both share similar features with water TPD on an O pre-covered surface [19]. A small amount of O pre-coverage is known to enhance partial dissociation significantly [15]. However, atomic oxygen alone cannot explain the observed changes fully (see the Discussion section). Therefore, we consider the new C/A2 peak at ~161 K which develops for higher photon dose (Fig. 1(a)) as a desorption peak for EUV damaged water layer which consists of water, partially dissociated water and possibly atomic oxygen. These water fragments might influence the adsorption and desorption of intact water. More specifically, the broken OH bonds can weaken the hydrogen bonds in the water layer, which reduces clustering and favours diffusion to the metal surface [12]. Moreover, because the C peak shifts continuously into the temperature range where A2 starts to desorb, we can also see this as an evidence for diffusion of water from the multilayer to the first layer on the Ru surface. To support this hypothesis, we point out that the surface coverage of water drops from 1 ML to 0.5 ML at the highest EUV fluence, leaving enough adsorption sites for the multilayer water to be re-adsorbed at the surface. The re-adsorption could take place during the TPD ramp or the exposure. However, it is most likely that this process happens during the exposure. Since the heating rate during each TPD measurement is 1 K/s, it only requires about 60 s to heat up the surface from 80 K to 140–150 K. This amount of time might be insufficient for diffusion. As shown in the STM experiment [26], significant removal of the high-lying water only appears after 30 min annealing.

3.2. TPD of CWB

Compared to ASW, the CWB exhibits some similarities. As shown in Fig. 1(b), exposure to EUV promotes the dissociation of water, as evidenced by the growth of the A1 peak at low exposures (see Fig. 2(b)). From the disappearing of the A2 peak, it suggests that the bilayer is converted to partially dissociated overlayer at fluence in excess of 5.7×10^{17} photons/cm^2. On the other hand, the A1 peak marks a much smaller change from 2.7×10^{17} to 5.7×10^{17} photons/cm^2, which appears as a flat plateau in Fig. 2(b), similar to ASW in Fig. 2(a) from fluence 1.2×10^{17} to 2×10^{17} photons/cm^2.

Unlike the ASW case, the C peak is missing in the CWB TPDs, because water is dosed above the desorption temperature for multilayer water. The CWB is already a well ordered structure, which results in less variations in the evolution of the A1 and A2 peaks. The A1 peak of CWB remains at saturation coverage of 0.45 ML, while the A1 peak of ASW reduces to 0.4 ML after reaching the saturation coverage of 0.5 ML. In Fig. 2(b), the A2 peak area is constantly dropping compared to a slowing-down between 2.4×10^{17} and 3.9×10^{17} photons/cm^2 for ASW (A2 + C) in Fig. 2(a). Overall, after A1 has reached saturation, the peak areas of CWB (A1 and A2) oscillates apparently less than ASW (A1 and A2 + C). The coverage changes of CWB appears to be more consistent in Fig. 2(b), which suggest that the formation of the partially dissociated layer is more direct without the interference of the multilayer.

Since a multilayer is absent, separate coverage for the A2 peak can be obtained. This allows us to evaluate the competition between partial dissociation and desorption of water from the changes of the A1 and A2 peak areas, respectively. In Fig. 2(b), Up to fluence of 2.7×10^{17} photons/cm^2, only small decreases occur in the total amount of water on the surface. In this region, one thirds of the molecular water is converted into partially dissociated water. As a result, surface coverage of water drops slower than the A2 peak. From EUV fluence of 2.7×10^{17} to 5.7×10^{17} photons/cm^2, the A1 peak is reaching saturation coverage. Meanwhile, the A2 peak still decreases constantly due to desorption/dissociation. The total amount of water on the surface also marks more drop in this fluence range.

The shifts in the peak desorption temperatures are clearly visible in Fig. 3. The A1 peak first increases from 226 K to 235 K between doses of 0 and 2.7×10^{17} photons/cm^2. At doses higher than 2.7×10^{17} photons/cm^2, the peak gradually returns to its original temperature. The A2 peak, however, shows a larger difference. The peak position reaches the lowest point 169 K at 4.1×10^{17} photons/cm^2. Then, it becomes almost invisible at 5.7×10^{17} photons/cm^2.

The desorption temperature of the CWB peaks provides a good indication of the waters surface structure and binding before it leaves the surface. It is clearly seen in Fig. 1(b) that the peak desorption temperature of the molecular layer moves towards that of multilayer water, which we also observe in the ASW case. This may indicate that intact water is becoming less stable on the Ru(0001) surface. Similar result can be found on water TPD on H pre-adsorbed Ru(0001) surface [15], where pre-adsorbed H destabilizes adsorbed water layer and cause water to desorb at a lower temperature [15]. As atomic H is one of the dissociation product of water, it can accumulate on the surface and destabilize the intact water [15].

Following the stoichiometry of water dissociation, we can predict the coverage of atomic H after exposure. The reaction $2H_2O \rightarrow H_2O + OH + H$ produces one H per two water molecules [15], which gives 0.22 ML atomic H coverage at the highest fluence 5.7×10^{17} photons/cm^2. The desorption temperature of hydrogen molecule is higher (from 260 K to 450 K) than the partially dissociated water ($H_2O + OH$). It is then more favourable for atomic H to desorb as water rather than H_2. This is also consistent with the small increase (15%) of H_2 desorption signal we observe after exposure.

3.3. Reaction cross sections

Due to differences in excitation mechanisms, electron and photon induced processes often have different reaction cross sections. The reaction cross sections can be considered as a signature for each reaction. We adapt the definition of reaction cross section for direct excitation in Ref. [11], in which the photon cross section σ (cm^2/photon) is defined as

$$\sigma = -ln\frac{\theta}{\theta^0}/n_{ph} \quad (1)$$

where θ and θ^0 are the remaining coverage and the initial coverage of the adsorbate, respectively, and n_{ph} is the photon fluence. By plotting the relative coverage θ/θ^0 against the fluence, we can obtain the reaction cross section from the slope of the linear fitting.

By plotting the total TPD signal as a function of EUV-dose on a semi-logarithmic scale (see Fig. 4), the cross section for water loss is obtained from the slope. We do notice that there is an induction period when significant exchange (up to 70% increase in peak area) between A1 and A2 peak takes place. However, in the same series of EUV exposures, only small amount (~6%) of water is lost. The cross section we obtained is, thus, an average from fluence 0 to 5.7×10^{17} photons/cm^2 and 7.3×10^{17} photons/cm^2 for CWB and ASW, respectively. From Fig. 4, the water loss cross sections [6,28] for ASW and CWB are found to be $9 \pm 2 \times 10^{-19}$ cm^2 and $5 \pm 1 \times 10^{-19}$ cm^2, respectively.

The relative stability of the water layers can also be compared via their water loss cross sections. Despite the fact that CWB is irradiated at higher temperature, the CWB appears to be more stable on Ru(0001)

Please cite this article as: F. Liu, et al., Surf. Sci. (2015), http://dx.doi.org/10.1016/j.susc.2015.09.009

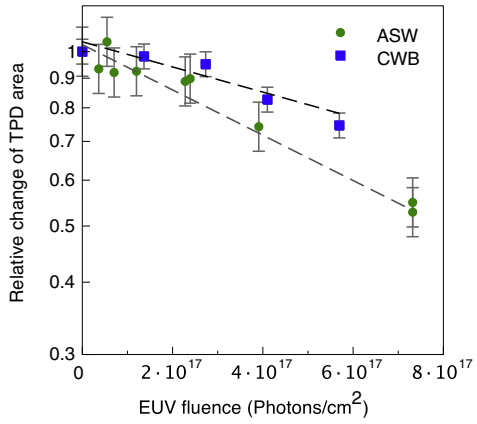

Fig. 4. Semi-logarithmic plot of the relative change of the integrated TPD spectra as a function of EUV fluence. The TPD spectra are obtained from EUV exposed ASW and CWB. The dashed line represents the linear fit of the data points. The resulting cross section deduced from the slope of the dashed line is 9×10^{-19} cm^2 and 5×10^{-19} cm^2 for ASW and CWB, respectively.

compared to ASW, based on the smaller water loss cross section. The greater stability of the CWB is possibly related to chemisorption on Ru and the bilayer geometry of the layer, which has three H-bonded neighbours per water molecule [13]. The hydrogen bonding in the bilayer significantly stabilizes water, therefore, hampers desorption. As CWB is also chemisorbed, excitations can be quenched by the substrate.

The reduction of the TPD signal is partially due to the partial and complete dissociation of water and partially due to desorption of water and water fragments during exposure. Fully dissociated water that cannot recombine to form a water molecule during the TPD ramp will remain on the surface as atomic oxygen and hydrogen. The dissociation pathway most likely follows $H_2O \rightarrow H + OH \rightarrow 2H + O$, or by one step dissociation $H_2O \rightarrow 2H + O$.

The reaction product atomic O can then oxidize the surface. The significance of the oxidation reaction is then given by the amount of atomic oxygen left on the surface. An oxygen TPD is performed directly following the water TPD to determine the amount of oxygen adsorbed on the Ru(0001) surface. Fig. 5 shows the atomic O coverage resulting from EUV induced full dissociation of water, which includes the measured small amount (0.003 ML) of oxygen due to complete thermal dissociation of water on Ru(0001) [6,15,25].

As with the water TPD spectra, a cross section for the photo-induced reaction $H_2O + Ru \rightarrow RuO + 2H$ was obtained by the same method used for the water loss cross section. In the calculation, the loss of water coverage is replaced by O coverage. To exclude the O coverage due to

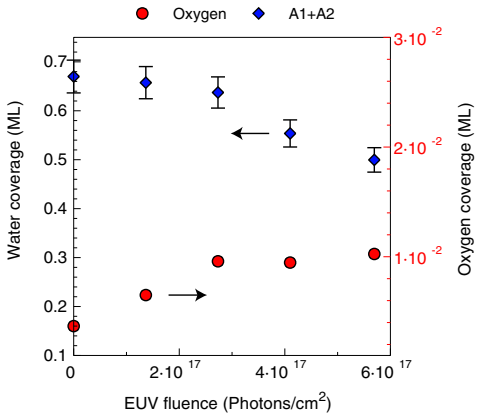

Fig. 5. Post-irradiation water (left axis) and oxygen (right axis) coverage after irradiation of CWB/Ru(0001). The coverage of water (A1 + A2) is reproduced from Fig. 2(b) for comparison.

thermal dissociation, we subtract each point by 0.003 ML from thermally dissociated water. The data is then linearly fitted in a semi-logarithmic plot, in which the slope of the fitted line yields the cross section. The cross section for the combined processes of full dissociation and O adsorption was found to be 2×10^{-20} cm^2, which is about 25 times smaller than the water loss cross section obtained from Fig. 4. Consequently, complete dissociation only partially explains the reduction of the integral TPD signal observed in Fig. 2, meaning most of the decrease in post-irradiation water desorption can be attributed to desorption of water (fragments) during EUV exposure.

4. Discussion

4.1. Increase in A1 peak

As suggested by many studies, understanding the structure and kinetics of the water–metal interface is still a challenging task [6,15]. Although much progress has been made over the years, there are still open questions on the water–Ru interface. One difficulty is the interpretation of the TPD spectrum of water. Based on the existing experimental results on water/Ru(0001) interface, the A1 peak increase can be originated from many causes. We will discuss a few of the plausible causes.

First of all, as suggested by Faradzhev [6], the increased A1 peak can be due to EUV and SE induced layer conversion of intact water to partially dissociated water. The amount of dissociated water is increased, therefore, less intact water is available to desorb at lower temperature. However, although rapid interchanges are observed for the A1 and A2 peaks, we do not observe a similar effect on the multilayer peak, which means the multilayer can undergo a different process than the layer underneath it. For example, desorption has a much smaller (about 7–10%) cross section than layer conversion [6]. Since the multilayer has no direct contact with the Ru surface, it cannot be converted into the partially dissociated phase. Therefore, desorption might be dominant inside the multilayer.

Secondly, the increase in the A1 peak can be O adatom related. As pointed out by Clay et al., surface impurities can influence the adsorption of water [15]. It has been shown that, by predosing the Ru surface with 0.04 ML of O, the A1 peak is increased by 50%. However, using the reaction cross section obtained above, no more than 0.01 ML of EUV produced oxygen can be expected on the surface. This coverage is insufficient to explain the entire increase of the A1 peak.

Thirdly, the water molecules on the Ru surface at 80 K form a hydrogen-bonded network. Radiation by EUV or electrons can have a profound influence on this network. Indeed, at photon excitation energy of 92 eV, the predominant desorbing products from the ice layer are H^+ and H_3O^+ [29,30]. With H^+ and H_3O^+ leaving the surface, hydroxyl groups are created inside the water layer. Although desorption of hydroxyls is not detected, it is still an open question on how this will change the competition between desorption/dissociation during the TPD ramp. Nevertheless, we expect it to have an effect similar to surface atomic oxygen on the thermal dissociation, which leads to increase in the A1 peak.

4.2. The role of SE

Although we irradiate water with EUV, the resulting reactions could be due to processes induced by both photons and secondary electrons [4,7,11,30]. In surface photochemistry, direct photon induced chemistry is only a special case [11], in which excitations from the substrate does not play a role. On the opposite, the adsorbate could as well be transparent for the excitation wavelength. Instead of photons, the SE from the substrate drives all the surface reactions. An electron counterpart of the photon cross section can be likewise formulated as

$$\sigma_e = -ln\frac{\theta}{\theta^0}/n_{se} \quad (2)$$

where σ_e is the electron cross section (cm^2/electron) for the SE induced reaction. Since the electrons are produced by absorption of photons, the number of electrons n_{se} depends on the number of the photons and the secondary electron yield of the substrate, which is defined as

$$Y_{se} = n_{se}/n_{ph}. \quad (3)$$

Replacing n_{se} in Eq. (2) by $Y_{se} * n_{ph}$, the effective photon cross section is given by

$$\sigma_{ph}^{se} = \sigma_e * Y_{se}. \quad (4)$$

In a more general case, such as in EUV surface photochemistry, both direct excitation and indirect excitation are present. Identifying the role of the electrons is not straightforward, since the secondary reactions due to the electrons cannot be separated from the photon induced reactions. Consequently, the quantity θ_0–θ, which is the coverage of the reacted adsorbate, is only measured as the sum of the two processes. Therefore, only the photon cross section was possible to be measured. However, the electron cross section σ_e can usually be obtained in a separate electron impact experiment [6]. By applying Eq. (4), we can estimate the partial cross section σ_{ph}^{se} for the secondary reactions to compare with the measured photon cross section σ. This comparison provides a way to justify the role of the SE in a photochemical reaction on a particular substrate.

Taking water dissociation for instance, the most probable pathway for SE to dissociate water is through dissociative electron attachment (DEA). To dissociate from a transitory anion state, water must capture resonantly an incoming electron with sufficient energy. For instance, the desorption yield of H^- for amorphous ice on Pt starts from 5 eV electron energy and peaks at 6.5–7 eV. Below 5 eV, the yield is too low to detect [31].

Roughly 50% of the SEs have an energy higher than 5 eV [32]. The high energy tail of the SEs extends to 20 eV. Therefore, a fraction of the SEs can be captured to desorb ions such as H^- and O^- [31]. The significance of this pathway can be estimated by electron cross sections. First of all, electron capture cross sections depend strongly on the energy of the electrons and the phase of water [33,34]. In the condensed phase, water has a charge trapping cross section of 1.8×10^{-17} at 7.5 eV, which is more than double that of the gas phase DEA value [35]. Taking this into account, the average cross section for H^- desorption from 5 eV to 12 eV is estimated to be $6 \pm 2 \times 10^{-18}$ cm^2. This value is the average of the gas phase values given in [35] and the condensed phase values given in [34]. The gas phase value is multiplied by an enhancement factor 2 [34] to match the condensed phase value before averaging.

The other half of the SEs has energy below 5 eV. Although the energy is too low to desorb ions, electron impact can still cause water loss on the surface. The experimental cross section for water (D_2O) loss is 7×10^{-18} cm^2 per 5 eV incident electron [6]. However, the results in [6] were inconclusive about the exact desorption product. It was assumed that water molecules were desorbed, based on the absence of detectable levels of atomic oxygen.

We listed both photon (experimental) and SE (estimated) cross sections in Table 1. As shown in the table, SE cross sections only add up to less than half of the observed water loss cross section and oxidation cross section in our experiment. This is mainly due to the low SE yield (0.02) for Ru. However, we should point out that the SE yield only accounts for the electrons that have energy above the vacuum level of Ru [32], which is caused by a SE cut-off at the work function of the sample [36]. On the other hand, using two photon photoemission spectroscopy, charge transfer between metal and ASW interface is observed for energies 2.0–4.0 eV above the fermi level [37], which suggests that a certain amount of electrons can be injected into the water layer. It has been reported that hot electrons above conduction band of ASW (3 eV on Ru) can cause desorption of water molecules [38]. Nonetheless, hot electron induced desorption of water can be excluded from our experiment, since our excitation density is orders of magnitude smaller than the observed threshold [38]. Based on the considerations above, we attribute the remaining part of the water loss cross section to photon induced desorption of water and water fragments.

Table 1
Photon cross sections for EUV and (estimated) SE induced water dissociation on Ru(0001).

Reaction	EUV (CWB, 92 eV)	EI (5 eV)[a]	DEA σ_{max}[b]
Water loss	5×10^{-19} cm^2	1.4×10^{-19} cm^2	H^-: 6×10^{-20} cm^2
Oxidation	2×10^{-20} cm^2	$<3.2 \times 10^{-20}$ cm^2	O^-: 2×10^{-21} cm^2

[a] Electron cross sections from Ref. [6] multiplied by SE yield 0.02.
[b] Electron cross sections from Refs. [35] and [34] multiplied by SE yield 0.01 for SEs with energy higher than 5 eV.

On the other hand, Ru is a good catalyst for dehydrogenation. The activation energy for conversion of an intact water overlayer to the partially dissociated water overlayer on Ru(0001) is just 0.64 eV [14]. 5 eV electrons can convert intact water to a partially dissociated overlayer efficiently with a cross section around 1×10^{-16} cm^2 for D_2O. Multiplied by the SE yield 0.02, the photon equivalent value is 2×10^{-18} cm^2, which lies closely to the photon absorption cross section at 92 eV [39]. Therefore, it is very likely that the conversion to the partially dissociated layer is entirely dominated by SE on Ru.

4.3. Oxidation cross section

Finally, we comment on the total reaction kinetics of EUV + water/Ru → RuO_x. The reaction cross section is rather small compared to the photon absorption cross section of water in gas phase [39]. However, dissociation to oxygen is a much slower process than dissociation to hydrogen in condensed phase water [30]. For instance, the DEA cross section for H^- is 30 times larger than for O^- (See Table 1). The surface oxygen was undetectable by X-ray photoelectron spectroscopy (detection limit 0.01 monolayer) after an electron dose of 4 e/molecule [6]. This puts an upper limit for the electron cross section for complete dissociation, which is at least two orders of magnitude smaller than that for conversion from intact to partially dissociated water on Ru (Table 1).

5. Summary

The EUV-induced photochemistry of water on Ru(0001) has been studied. The main reaction products left on the surface were determined to be partially dissociated water (OH + H) and a small fraction of atomic oxygen. We observe that, under EUV radiation, water rapidly forms a partially dissociated overlayer on Ru surface. Dissociation of water and desorption of the reaction products also reduce the total amount of water on the surface. From the reduction of the water coverage, the primary dissociation pathway of water under EUV radiation is identified to be $H_2O \rightarrow OH + H$. The reaction cross sections for loss of water were measured to be 9×10^{-19} cm^2 and 5×10^{-19} cm^2 for ASW and CWB, respectively. The smaller cross section for CWB indicates that it is more stable under EUV radiation. The complete dissociation of water ($H_2O \rightarrow 2H + O$) is also identified by detection of adsorbed oxygen after the exposure. The cross section for this reaction is measured to be 2×10^{-20} cm^2. The role of the SE was also investigated. Because of the relatively small SE yield of the Ru crystal, we estimate that SE has only minor contributions in the reactions which cause water loss and oxidation.

Acknowledgements

This work is part of the research programme Controlling photon and plasma induced processes at EUV optical surfaces (CP3E) of the Stichting voor Fundamenteel Onderzoek der Materie (FOM) with financial support from the Nederlandse Organisatie voor Wetenschappelijk

Onderzoek (NWO) under the Grant No. i23. The CP3E programme is co-financed by Carl Zeiss SMT and ASML, and the AgentschapNL through the EXEPT programme.

References

[1] V. Bakshi, EUV Lithography, SPIE Press; John Wiley, Bellingham, Wash. Hoboken, NJ, 2009.
[2] M. Neisser, S. Wurm, Adv. Opt. Technol. 1 (2012) 217.
[3] P. Maksyutenko, T.R. Rizzo, O.V. Boyarkin, J. Chem. Phys. 125 (2006) 181101.
[4] T.E. Madey, N.S. Faradzhev, B.V. Yakshinskiy, N.V. Edwards, Appl. Surf. Sci. 253 (2006) 1691.
[5] A. Al-Ajlony, A. Kanjilal, M. Catalfano, S.S. Harilal, A. Hassanein, Appl. Surf. Sci. 289 (2014) 358.
[6] N.S. Faradzhev, K.L. Kostov, P. Feulner, T.E. Madey, D. Menzel, Chem. Phys. Lett. 415 (2005) 165.
[7] J. Hollenshead, L. Klebanoff, J. Vac. Sci. Technol. B Microelectron. Nanometer Struct. 26 (2006) 118.
[8] X. Zhu, Annu. Rev. Phys. Chem. 45 (1994) 113.
[9] K. Andersson, A. Nikitin, L.G.M. Pettersson, A. Nilsson, H. Ogasawara, Phys. Rev. Lett. 93 (2004) 196101.
[10] I.J. Malik, J. Hrbek, J. Vac. Sci. Technol. A 10 (1992) 2565.
[11] X.L. Zhou, X.Y. Zhu, J.M. White, Surf. Sci. Rep. 13 (1991) 73.
[12] M.A. Henderson, Surf. Sci. Rep. 46 (2002) 1.
[13] G. Held, D. Menzel, Surf. Sci. 316 (1994) 92.
[14] A. Michaelides, A. Alavi, D.A. King, J. Am. Chem. Soc. 125 (2003) 2746.
[15] C. Clay, S. Haq, A. Hodgson, Chem. Phys. Lett. 388 (2004) 89.
[16] T.E. Madey, H. Albert Engelhardt, D. Menzel, Surf. Sci. 48 (1975) 304.
[17] B. Artur, N. Horst, J. Chem. Phys. 110 (1999) 3186.
[18] J.M. Sturm, C.J. Lee, F. Bijkerk, Surf. Sci. 612 (2013) 42.
[19] D.L. Doering, T.E. Madey, Surf. Sci. 123 (1982) 305.
[20] M.J. Gladys, A. Mikkelsen, J.N. Andersen, G. Held, Chem. Phys. Lett. 414 (2005) 311.
[21] S.Y. Li, J.A. Rodriguez, J. Hrbek, H.H. Huang, G.Q. Xu, J. Vac. Sci. Technol. A 15 (1997) 1692.
[22] J. Weissenrieder, A. Mikkelsen, J.N. Andersen, P.J. Feibelman, G. Held, Phys. Rev. Lett. 93 (2004) 196102.
[23] D.P. Woodruff, T.A. Delchar, Modern techniques of surface science, Cambridge Solid State Science Series. 2nd edition, Cambridge University Press, Cambridge; New York, 1994.
[24] S. Messaoudi, A. Dhouib, M. Abderrabba, C. Minot, J. Phys. Chem. C 115 (2011) 5834.
[25] G. Pirug, C. Ritke, H.P. Bonzel, Surf. Sci. 241 (1991) 289.
[26] S. Maier, I. Stass, J.I. Cerda, M. Salmeron, Phys. Rev. Lett. 112 (2014).
[27] P.A. Redhead, Vacuum 12 (1962) 203.
[28] X.Y. Zhu, J.M. White, M. Wolf, E. Hasselbrink, G. Ertl, J. Phys. Chem. 95 (1991) 8393.
[29] K.W. Kolasinski, J. Phys. Condens. Matter 18 (2006) S1655.
[30] D. Coulman, A. Puschmann, U. Höfer, H. Steinrück, W. Wurth, P. Feulner, D. Menzel, J. Chem. Phys. 93 (1990) 58.
[31] X. Pan, H. Abdoul-Carime, P. Cloutier, A.D. Bass, L. Sanche, Radiat. Phys. Chem. 72 (2005) 193 (Christiane Ferradini Memorial Issue).
[32] B.V. Yakshinskiy, R. Wasielewski, E. Loginova, T.E. Madey, Emerging Lithographic Technologies XI, Pts 1 and 2 6517 2007, p. Z5172.
[33] W.C. Simpson, T.M. Orlando, L. Parenteau, K. Nagesha, L. Sanche, J. Chem. Phys. 108 (1998) 5027.
[34] A.D. Bass, L. Sanche, Radiat. Environ. Biophys. 37 (1998) 243.
[35] P. Rawat, V.S. Prabhudesai, G. Aravind, M.A. Rahman, E. Krishnakumar, J. Phys. B At. Mol. Opt. Phys. 40 (2007) 4625.
[36] A. Shih, J. Yater, C. Hor, R. Abrams, Appl. Surf. Sci. 111 (1997) 251.
[37] J. Stähler, C. Gahl, U. Bovensiepen, M. Wolf, J. Phys. Chem. B 110 (2006) 9637.
[38] E.H.G. Backus, M.L. Grecea, A.W. Kleyn, M. Bonn, J. Phys. Chem. B 111 (2007) 6141.
[39] J.W. Gallagher, C.E. Brion, J.A.R. Samson, P.W. Langhoff, J. Phys. Chem. Ref. Data 17 (1988) 9.

Please cite this article as: F. Liu, et al., Surf. Sci. (2015), http://dx.doi.org/10.1016/j.susc.2015.09.009